



Potential of kite-borne photogrammetry for decimetric and kilometre square 3D mapping: an application for automatic gully detection

Feurer Denis¹, Planchon Olivier¹, El Maaoui Mohamed Amine², Boussema Mohamed Rached², and Pierrot-Deseilligny Marc³

¹IRD, UMR LISAH (INRA-IRD-SupAgro), F-34060 Montpellier


²El Manar University, National Engineering School of Tunis, LTSIRS, B.P 37, 1002 Tunis-Belvédère Tunis, Tunisia

³Université Paris-Est, IGN/SR, LOEMI, 73 avenue de Paris, 94165 Saint-Mandé, France

Correspondence to: Denis FEURER (denis.feurer@ird.fr)

Abstract. This work proposes an alternative method to answer the issue of quasi-exhaustive mapping of erosion features on kilometre square areas by remote sensing. This study presents a method to produce decimetric Digital Elevation Models (DEMs) with kite aerial photography and an algorithm to map gully erosion from these DEMs.

Kite aerial photography is robust and cheap in comparison to Unmanned Aerial Vehicles (UAVs). The use of such a simple apparatus is made possible if the flight angle of the kite is steady. Experimentation and modelling show that this goal can be reached with these two predetermined conditions: the right kite must be used in the right wind and the line must be light and thin. In our study, we used a 10m² framed delta kite in 4-5 Beaufort winds using a Dyneema® line of 1mm in diameter and 0.5g.m⁻¹ in weight for image acquisition on the day of experiment.

Within two successive flights, 752 images were acquired. The photogrammetric software used was Micmac, an open-source software written and maintained by the French national institute of geographic and forest information (IGN). It allowed to obtain DEM covering  km². Geographical reference was given by 8 ground points and 469 independent points were surveyed for validation. Estimated mean error on altitudes was 0.07m and standard deviation of this error 0.22m, for a 0.11m ground sampling distance.

In order to illustrate the potential of such detailed DEMs at the watershed scale, a simple gully detection algorithm was briefly described and implemented. ~~As with several others,~~ the method does not refer to the relationship between slope and drainage area but uses local convolution of the DEM. Considering a smoothed DEM as a proxy of the geomorphological process of gullies healing, proposed gully detection algorithm relies on subtracting smoothed DEM from the original DEM. The depth of each feature is then estimated and only the bulkier elements are kept as potential gullies. Despite our algorithm detecting undesired artefacts - most of them being man-made structures such as houses and roads - all gully heads and all channels are detected. Therefore results show the benefits of the production and use of decimetric DEMs on an entire kilometre square watershed with kite-borne imagery.



1 Introduction

Context

The production of high-resolution topographic datasets is of increasing interest throughout the geomorphological sciences (Bird et al., 2010; Fonstad and Marcus, 2010; Fonstad et al., 2013). We are currently witnessing a fast-moving ~~race towards~~ larger and higher-resolution DEMs. On the other hand, erosion remains a natural hazard for which fine scale monitoring on kilometre square areas remains difficult. ~~Such a race will hence greatly benefit erosion science.~~ Because the study of gully erosion requires detailed field surveys, research work must concentrate either on a few gullies with high-density topographic data, or on an entire gully system with coarser data. As a side effect, studies on gullies often concern large gullies of several metres in width and in depth, which evolve rapidly. They are often identified on aerial photographs, and their evolution in time is assessed ~~on in the long term~~ by comparing photographs taken at intervals of years (Nachtergaele and Poesen, 1999) or decades (Vandekerckhove et al., 2003; Campo-Bescós et al., 2013; Hayas et al., 2015).

In contrast, the monitoring of small gullies with rapid evolution is generally done manually by field survey. For example, Hancock and Evans (2006) have identified two hundred gully heads on a site of 200ha. Being on the field they could focus on small gullies. However, they were unable to monitor the evolution of such a large set of erosion features. Because of these metrological difficulties, the field study of gullies over a short term are those of large size with rapid development (see Rengers and Tucker, 2015, and many others cited in the comprehensive review of Vanmaercke et al., 2016). We believe that the reason why the community of erosion science focuses on large gullies with rapid evolution is not due to the special importance of these gullies, but simply to the ~~insurmountable~~ challenge of monitoring a large number of small gullies. Yet, their small size is compensated by their number and small gullies are possibly as harmful as large ones. More detailed DEMs would allow the monitoring of small gullies, the development of which is of crucial importance for agriculture. When such DEMs cover large areas, gullies can be studied at their scale of interest, which is the watershed.

There is hence a need for methods allowing fast (a few days of work), simple (usable with no prior technological knowledge) and affordable (in the order of 1000 euros for the hardware, and open-source software) way of mapping gullies of metric size on an entire small watershed, namely a few square kilometres. A DEM with decimetric resolution is required to delineate metric scale gullies. The area of interest is the watershed that includes the gullies, which is typically in the order of magnitude of a square kilometre. Mapping a few square kilometres at the resolution of some tens of centimetres will produce data of several hundred megapixels in size, which requires the use of latest image processing algorithms. In this introduction, we demonstrate that the combination of kite photography and Structure from Motion algorithms is a valuable choice in terms of feasibility and cost-effectiveness.

30 Structure from Motion (SfM)

Around a decade ago, researchers in photogrammetry started to use algorithms originally written for computer vision and robotics. They are referred to as structure from motion (SfM) algorithms. SfM consists of using a large number of images with a large overlapping ratio to calibrate simultaneously the internal (image deformation) and external (camera position) parameters



of the entire photogrammetric project. Contrary to older methods, this step requires no special target on the field and no previous knowledge of the camera settings. SfM relies on the SIFT (Scale-Invariant Feature Transform) algorithm (Lowe, 2004). SIFT recognises thousands of special points in the images that can be associated with a numerical signature independent of the position of the feature in the image and of its scale. Thanks to their unique signature, the SIFT points can be blindly matched

5 between images, producing a huge amount of pairs of points on the basis of which the calculation of the camera calibration, relative position and pose is done in one step. The important point of the above is that SfM allows the automatic calibration of a virtually unlimited number of images with no intervention of the user, neither on the field to place artefacts for tie points, nor in the process of calibration. This simplified workflow has revolutionized photogrammetry, as quoted from Westoby et al. (2012): "The last decade has witnessed a technological revolution in geomatics that is transforming digital elevation modelling

10 and geomorphological terrain analysis". The SfM-based photogrammetric workflow is described in detail in their paper, as well as in Fonstad et al. (2013) and several others. Much software use SfM-based photogrammetry. The vast majority of them being oriented towards the calculation of 3D objects. Much fewer are specifically oriented towards the computation of DEMs. Even fewer are free or released at an affordable price. Among them is PhotoScan(R) by Agisoft (2014), with a price tag around five thousand euros for academic use. PhotoScan, which integrates the entire processing chain for the production of DEMs is more

15 and more widely used in the scientific community. Alternatively Micmac (Pierrot-Deseilligny and Paparoditis, 2006) is an open-source software written and maintained by the French national institute of geographic and forest information (IGN). Micmac encompasses the entire workflow with several unique features. One of the most important of them is the implementation of the dense matching algorithm used by IGN in the calculation of all their commercial products. Photoscan(R) and Micmac(R) were compared with each other (e.g. Jaud et al., 2016) and proved equally satisfying. PhotoScan is more straightforward to use but its

20 source code is not open; MicMac is recommended for experimental users as it is more flexible. Besides these straightforward solutions are a number of hybrid workflows, as mentioned by Rango et al. (2009). For example, Bryson et al. (2013) used not less than seven types of software from various sources, including three customized implementations. Another more commonly used hybrid solution is the association of Bundler (Snavely et al., 2006) and PMVS2 (Furukawa and Ponce, 2010). In the field of geosciences, several SfM-based photogrammetric projects can be found in the literature that are remarkable either by

25 the number of images processed (several hundreds), by the size of the study site (several square kilometres) or by the ground resolution of the DEM (sub-centimetric). Harwin and Lucieer (2012) used 105 images to calculate a DEM of a 5ha study site with a resolution of one to three centimetres and a precision of 2.5cm to 4cm. Bryson et al. (2013) used a small UAV based on a kite with a small motor and an autopilot. They surveyed a 200m by 30m large area. They calculated sub-centimetric details based on a set of 295 images. Several studies used orthophotography calculated at decimetric resolution on areas of several

30 square kilometres. In most cases, the DEM was calculated in the principal objective of producing the orthophotography. In such cases, the DEM was calculated at much coarser resolution. **To our best knowledge, the calculation of a decimetric DEM on an area larger than a square kilometre is unprecedented in the field of geoscience.**



Kite aerial photography (KAP)

In their book, Aber et al. (2010) did not dedicate more than a few pages to the kite and the indications provided are limited to generalities. This reflects what is most commonly found in the literature. In effect, it is relatively easy to take pictures from a kite at heights of below 100 m because the camera's orientation can be seen. Lorenz and Scheidt (2014) even wisely suggested to use this system without a special objective in mind, simply for the sake of curiosity and documentation. From a general point of view, the kite appears to be particularly adapted to document and/or measure detailed features on the ground. For example, back in 2009, Marzloff and Poesen (2009) succeeded in making a detailed survey of a gully head in Spain with a kite and a consumer-grade camera. Other examples of such detailed surveys are many. However, much more can be done by kite if one considers that the kite is on par with, or better than, electrical UAVs in every of the six desirable qualities mentioned by Nex and Remondino (2014): payload, wind resistance, minimum speed, flight autonomy, portability and landing distance (although the performances of electrical UAVs are increasing rapidly). Moreover, kite has two key advantages over UAVs which justifies our choice. First, a kite is easier to fly than an UAV. Virtually everyone can fly a kite after a demo and some advice. Second, the administrative regulations on kite aerial photography are much more permissive than those for photography from an UAV. Especially, in several countries in Northern Africa, where our study site is located, importation of radio-controlled equipment is either forbidden or an administrative hassle. All these reasons make kites valuable alternative platform for very high resolution remote sensing and, as pointed by Duffy and Anderson (2016), may lead to a "revival" of kites in a field largely led by RPAS technology.

Goal

In this study, we demonstrate the use of kite photography and SfM-based photogrammetry to measure a DEM at 11cm of resolution over a study site of 3km². The DEM is devoted to the systematic study of gully erosion over the entire watershed. Preliminary results on the delineation of gullies are presented to illustrate the potential of decimetric DEMs at large scale. We first demonstrate how and why a precise positioning of the kite can be achieved. We then present the resulting DEM along with an assessment of its overall quality. Although the paper is primarily a description of the method used to measure and calculate high-resolution topography at large scale, a brief example of application is presented at the end to demonstrate the potential of such data for the delineation of erosion features.

2 Material and methods

2.1 Study site

The study site is the Kamech watershed, Tunisia (Figure 1-b), which is a small experimental watershed of 2.63km², located on the Cape Bon, a peninsula in the North East of Tunisia (Figure 1-a). Detailed description can be found in Mekki (2003), Mekki et al. (2006), and Raclot and Albergel (2006). Elevation ranges between 80 and 100m. Slopes can locally exceed 100% and the landscape is crossed by several hundred gullies. The outlet of the watershed is a small hill dam with a reservoir of

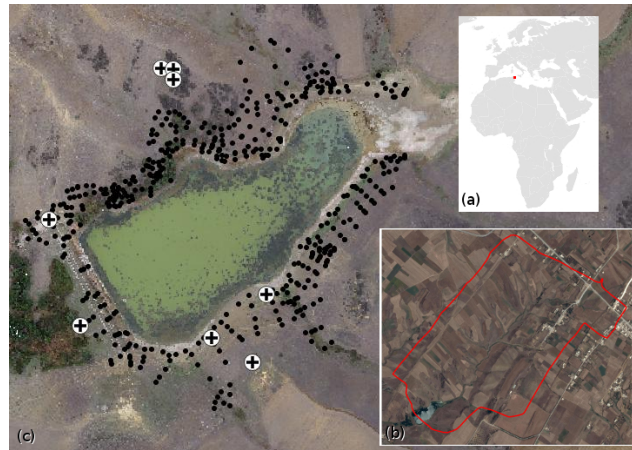


Figure 1. Location of the Kamech test site and available ground truth data. (a) Location of the Cape Bon, in the north east of Tunisia; (b) close-up on the Kamech watershed, 263ha, delineated in red; (c) close-up on the available ground truth data: ground control (crosses) and validation points (black dots)

30 140 000m³ at the time of construction (Figure 1-c). The reservoir is monitored since 1994 as part of a research agreement between the Direction for Soil and Water Conservation at the Tunisian ministry of agriculture (DG ACTA/CES, Tunisie) and the French Institute of Research for Development (IRD) and is one of the two sites of the research observatory OMERE (<http://www.obs-omere.org>). The substratum of this test site is mainly composed of intercalations of marl and clay zones and sandstone layers. These layers have a ~~global~~ inclination of around 30 degrees. The right-bank side of the catchment has a slope ~~globally~~ parallel to this inclination and presents mainly marly layers. Hence most gullies have developed on this side. Quantitative monitoring of erosion on this site is mainly focused on individual gullies considered as representative of the general active processes and has been done with classical topographic methods (see Khalili et al., 2013, ~~for detailed results~~).

2.2 Kite-based image acquisition method

A steady flight angle

10 The image acquisition protocol lies on the following hypothesis: with a very stable kite as a payload carrier, embarked camera remains stationary in relation to the kite operator. As a consequence, the "flight ~~plan~~" is a simple translation of the operator's movement. Hence the "flight plan" can be prepared and followed on ~~ground~~, without any necessity of having a remote control of the platform ~~nor~~ a downlink giving information about the carrier position. The operator only needs to know flight angle and kite line length (Figure 2).

15 Flight altitude is controlled by line length. The line is hence graduated every 10m on the first 100m and then every 50m with a simple colour/thickness coding system. A comparable approach is used by Bryson et al. (2013), with fewer constraints on the acquisition protocol due to the low altitudes. In the case of the method described in this paper, whose aim is to seamlessly

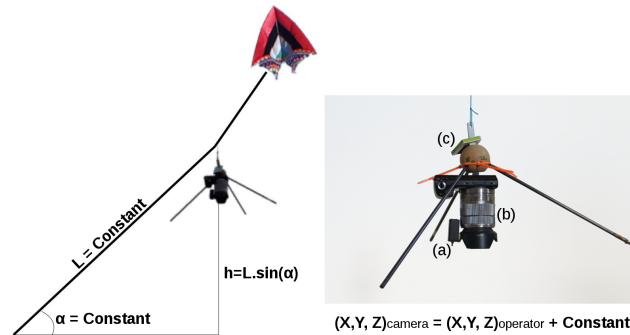


Figure 2. Left: schematic principle of acquiring images by kite with a steady flight angle. Right: Tripod with camera (a) intervaillometer ; (b) camera ; (c) GPS.

acquire images on kilometre square wide areas, flight angle stability had to be carefully investigated and its mean value properly estimated.

Evaluation of the average flight angle and its steadiness for each kite and for different operating conditions has been done with two complementary approaches.

5 First, each kite was flown within different wind conditions and with different line lengths. Camera and operator positions were logged with a standalone **GPS data logger** (Figure 2-c). These logs have then been used to compute effective flight angles. This information also allowed us to check for the ideal windrange in which the kite remains stable and with a steady flight angle.

Besides experimental data, numerical simulations of line shape and kite position have been done for different wind condi-
10 tions, from $3\text{m}\cdot\text{s}^{-1}$ to $11\text{m}\cdot\text{s}^{-1}$, which roughly corresponds to Beaufort winds from 3 to 7. Use of Beaufort scale is preferred in field as it can be estimated from direct observation and does not require any anemometer. The simulations compared two 300m kite lines with two different materials: a Dyneema® line weighing $0.1\text{g}\cdot\text{m}^{-1}$ and a polyester line with a weight of $1\text{g}\cdot\text{m}^{-1}$. For the sake of simplicity, simulations have been done with the same diameters for both lines. However, as the Dyneema®
15 line is stronger than polyester, it is usually used with smaller diameters. For each line type, simulations compared the ideal case (no draft and lines with no weight, leading to the kite line being straight) with the more realistic scenario where the line is bowed by these two physcial phenomena. Effect of line length has also been assessed, both with these simulations and by experimentation. Empirical observation was carried out: using a thin and light line, notably, the line weight and draft should have a negligible impact on effective flight angle, even with long lines.

Robust and simple equipment

20 Criteria for choosing the material were cost, robustness, in-flight reliability and easy set up. The whole equipment is constituted by the platform itself, the rig attached below, a camera and a small GPS (Figure 2)



For the platform, framed delta kites were used. They have been chosen within a large variety of kites because of their flight qualities (stability and high flight angles), easy to mount - with no need for adjustment on the field - and fair payload. In this study, two delta kites, one of 4m² and another one of 10m² have been used. The line used for all experimental setups is a thin and light 90kg Dyneema® line.

The rig is a simple tripod hung down a long line forming a simple pendulum (Figure 2). The rig is fixed to the kite line some tens of metres apart from the kite itself so that the rig is less sensitive to kite movements. In addition, using a long line for the pendulum ensures low-frequency movements of the rig around the vertical position. Finally, acting in the wind as a vane, the tripod allowed for a natural aerodynamic stabilisation of the yaw angle. Even if not necessary for image processing - variable yaw angle can even be interesting for specific applications - stable yaw angle can however be interesting for manual images inspection after flight.

The camera was chosen as a compromise between weight, image quality and cost. A good compromise found at the time of the experiment was the Sony NEX-5N, which allows us to take 16Mpix images with fixed focal and disabled image stabilizer (Figure 2-b). A GentLED-Auto intervallometer has been used to automatically trigger the camera at given time intervals (Figure 2-a).

Two autonomous QSTARZ BT1400S GPS loggers were used, one attached onto the camera (Figure 2-c) and the second on the kite operator. This positional information has been gathered in order to develop and refine the image acquisition protocol at first and then to check its operational application.

2.3 Field and image data

Four flights were done on this site during three days with various conditions of wind, and with either one of the two available kites, depending on wind conditions.

As a recurrent operation of the OMERE observatory, bathymetry and topography of the reservoir ~~has been done~~ a few weeks before image acquisition. From this dataset, eight points (cross marks on Figure 1) could be used as Ground Control Points (GCPs) to give spatial reference as an input to the photogrammetric image processing step described in the following section. Additionally, 469 points measured around the reservoir were used as independent validation points. Due to the fact that this dataset was not constituted with a view to validate a SfM DEM, some points of the original data set had to be removed: these points were located under or too close to trees and would have led to a bad estimation of DEM error. All these points were measured with a Topcon GR-3 RTK DGPS with a given altimetric and planimetric accuracy of 1.5cm. Further estimation of altimetric accuracy with the same instrument was however proven to be closer to 3cm. Validation points were not used to compute the 3D model and were kept for independent quality assessment of the DEM.

Once the kite flight behaviour has been characterised - in particular effective flight angle - the last flights were used to obtain a quasi-complete coverage of the Kamech catchment, with a maximum flight altitude of 500m leading to a maximum estimated ground pixel size of 0.13m. In total, 752 images have been used to cover an area of 318ha (see Table 1 for a summary of all these figures). However, the very upstream part of the catchment could not be covered for security reasons linked to the



Table 1. Flight characteristics and data collected

Flight type	Calibration	Acquisition
Estimated Beaufort	3 to 7	4-5
Kite used	4 m ² & 10 m ²	10 m ²
Flying heights (m)	120 to 600	120, 300, 500
Line lengths (m)	150 to 700	150, 360, 600
GCPs	-	8
Validation points	-	469
Focal length (mm)	-	18
Sensor size (mm)	-	23.4x15.6
Images used	-	752
Max pixel size (m)	-	0.13
Total covered surface	-	318 ha

presence of a power line. More area - downstream and outside the catchment - could be reached, which explains that the total covered area (318ha) exceeds the total area of the catchment (263ha).

2.4 3D model production

Many photogrammetric software are available on the market, either commercial or open-source. We used the open-source solution Micmac (Pierrot-Deseilligny and Paparoditis, 2006). Micmac has already been described in the introduction in its broad lines. It implements the dense matching algorithm used by IGN to calculate their commercial 3D products. It is a hierarchical, true multi-view algorithm. It is hierarchical in the sense that coarser grids are gradually refined by dividing by two the resolution of the DEM at each step, until the user-defined final step (generally, full resolution) is reached. It is a true multi-view algorithm in the sense that all the images that can see the point being calculated are taken into account in the same bundle adjustment for the calculation of each point in the DEM. Thus, altimetric and planimetric precision is of the order of magnitude of one pixel. Of course, other kinds of software are available with algorithms of similar quality. For more information about the different SfM software available and their comparison with MicMac, the reader is invited, for instance, to consult the works of Stumpf et al. (2015), Jaud et al. (2016) or Smith et al. (2016).

The Micmac process (Table 2) is typical of SfM algorithms. Two points have some consequences on the planning of field work. The first point is the memory limit of the calibration algorithm (a module called Tapas). In this module, all SIFT points pairs previously recognized and matched are loaded in memory at the same time. This creates a bottle neck in resource capacity, especially in consumer-grade computers. Although some possibilities of reducing the number of SIFT point now exist, projects with more than one thousand images remain difficult to calibrate.



Table 2. Typical Micmac pipeline

operation	command name	main options ; <i>limitations, remarks</i>
SIFT points computing and matching	Tapioca	choice of image resampling ratio ; <i>affects number of SIFT points</i>
image orientation and autocalibration	Tapas	model of lens distorsion ; <i>memory necessary to load the whole set of SIFT points calculated in all images</i>
raw mosaic of the area	Tarama	<i>used to have a quick result of the covered area</i>
manually drawing area of interest	SaisieMasq	
giving spatial reference	SaisieAppuis GCPBascule	<i>manual pointing of GCP positions ; spatial reference can be given from GCPs and/or from GPS</i>
dense matching	Malt	final DEM resampling ratio & regularisation parameters
orthophotography	Tawny	parameters for radiometric regularisation

After the SfM (i.e. SIFT points recognition and matching + bundle calibration) is done the two manual steps of the process are performed. Firstly selecting the area for dense image matching and secondly pointing at the exact position of the GCPs.
 15 Then the project has a cartographical reference and the dense matching can be launched. When GCPs are not available, the georeferencing of the project can be done with GPS data giving camera position at the time of image acquisition. The pipeline ends with the calculation of the DEM and the orthophotography. The DEM is calculated by tiles so that the memory requirements fit with the computer capabilities. The computer used is a laptop computer equipped with an Intel Core i7-3840QM CPU at 2.80GHz and 32 Gb of memory.

20 Another **point** has a direct implication in the project: because the images are taken at a height of several hundred metres, images have a rather poor 3D structure. The bundle calibration can fail at calibrating the intrinsic parameters of the camera, or fall into a false minimum. For this reason, it is always recommended to acquire a special set of images for the camera calibration. They can be taken from the ground if an adequate 3D scene is available, or by flying at low height over a well-defined relief such as buildings or natural geomorphic features. The calibration obtained separately can then be used in the
 25 bundle adjustment.

2.5 Gullies detection

In field, a gully forms a sharp depression which is discordant with the smoothness of the surrounding topography. Gully border is the limit between the zone with smooth topography and the steep slopes of the gully. This border can be numerically detected by comparing the actual landscape to a landscape represented by a filtered digital elevation model. Filter window size is chosen according to typical widths of study site gullies. For our experiment, the applied processing was a gaussian filter with a 10m standard deviation. Figure 3 shows the different computing steps of the gullies extraction method used. First, the topography

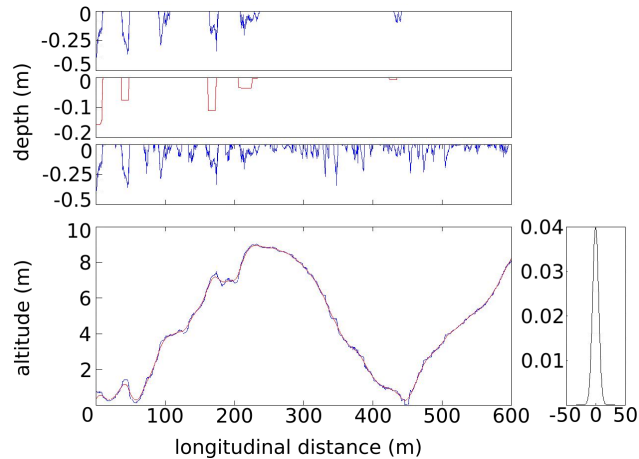


Figure 3. Principle of gullies contour detection. Right: the gaussian filter with 10m standard deviation. Left, from bottom to top: original (blue) and smoothed (red) topography ; raw negative differences between original and smoothed topography ; detection of possible gullies with a threshold on the depth of the element ; detected gullies

is smoothed ; then negative differences between original topography and smoothed topography are computed. This raw map of negative differences comprises a lot of noise, essentially a lot of little **zones** with low extent depressions. At this step, each detected zone is isolated and the depth of these features is computed. A threshold on the volume has been used to select which features are considered as gullies and which features are considered as noise. The residual noise was removed manually to obtain the final gullies map.

3 Results

3.1 Kite in-flight characteristics

Importance of kite line

Figure 4 shows the results of kite line shape simulation with different wind speeds, line characteristics and physical processes taken into account. This figure confirms three field observations: (i) with light and thin lines, the kite line is almost straight and the flying angle is maximal ; (ii) when the kite is flown with sufficiently strong wind, wind speed variation causes only small effective flight angle variations ; (iii) the latter observation is all the more true when the kite line is thin and light. In conclusion, using a thin and light kite line, and the kite adapted to the actual wind conditions at the time of image acquisition is mandatory for obtaining a steady flight angle.

Figure 5 shows the simulated flight angle as a function of the line length for Dyneema® line and polyester line. Not surprisingly, the figure shows that the flight angle drops with increasing line length. The drop is slight for the Dyneema® but critical for the polyester line, due to the stronger "banana" line shape effect observed in field and in Figure 4.

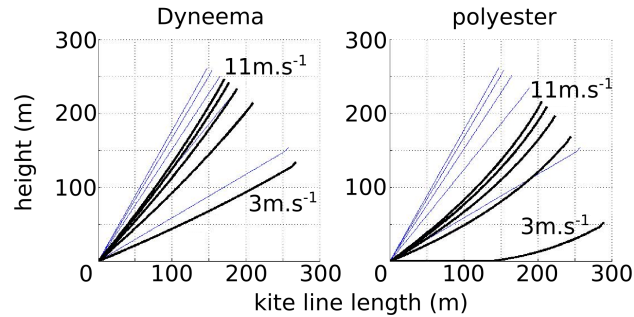


Figure 4. Comparison of the shape of 300m lines (black bold) with "ideal" (thin grey) ones on a kite flown under different wind conditions. "Ideal" lines are modelled as weightless and causing no drag. Left: Dyneema® line (0.1g.m^{-1}). Right: polyester line (1g.m^{-1}).

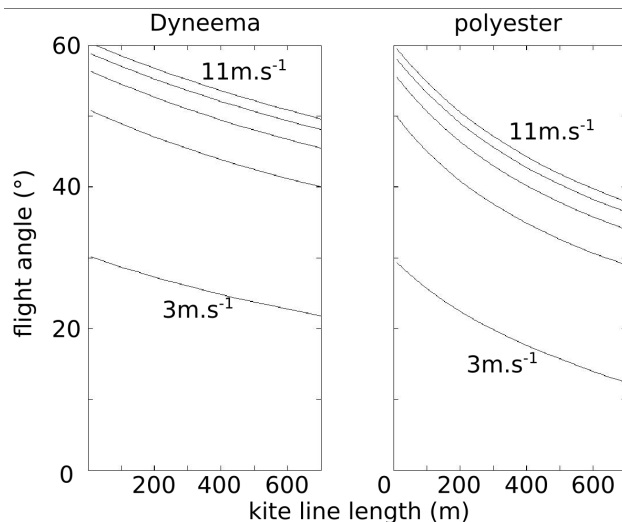


Figure 5. Simulation of the variation of the flight angle with the line length for different winds. Left: Dyneema® line. Right: Polyester line

Flight angle and windranges

Empirical observation, confirmed by the simulation results showed above, led us to choose the thinnest and lightest Dyneema® line whose strength would secure the payload. Considering that the drag of the kites is always less than twenty kilograms even in strong winds (otherwise a smaller kite - with lower drag - is used), the chosen strength was 90kg.

Figure 6 shows the measured effective flight angle for the two kites used with the Dyneema® line. Measured flight angles are summed up as min/max boxes for each flight. This figure confirms what was anticipated after Figure 5: the flight angle drops slightly but significantly with the line length, and this drop must be taken into account for the preparation of the field work. We also see that the smaller kite - which has a tail - flies at a significantly lower angle than the larger one. This figure also includes a flight where the wind strength was insufficient to fly the 10m^2 kite. Characteristics of this flight are represented

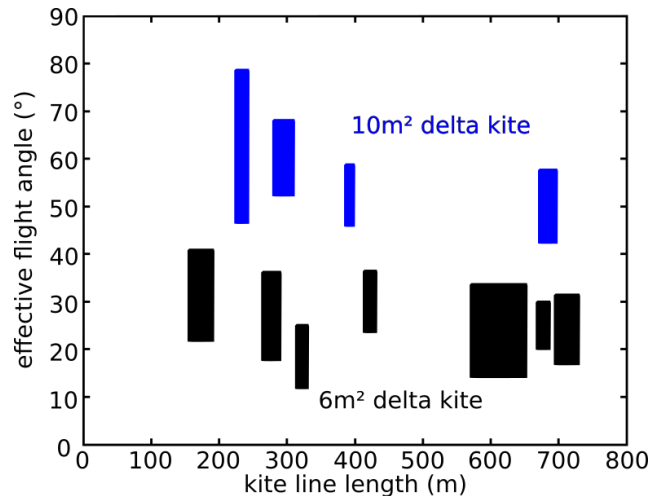



Figure 6. Observed flight angle for the two kites and various conditions of wind speed and line length.

by the leftmost blue box. This confirms that when the kite is not flown in the appropriate conditions, flight angles are far more variable 

Flight duration

The autonomy of the various equipment takes into account the autonomy of batteries and the size of the memory, both for the camera and the GPS. These must be known prior to operating the entire system. It happened that our system was limited by the battery of the camera when the following settings were used: 64Gb memory card, triggering set to one image acquisition every five seconds, and GPS logging frequency set at 1 Hz. In these conditions we could do flights of three and a half hours, yielding potentially more than 2500 images. This amount of images corresponds to a significantly high computation time and need of memory for full resolution processing on a consumer-grade computer but gives an idea of the mapping potential of this equipment, which can be counted in **gigapixels**.

3.2 3D model

The whole processing chain was fed with 752 images for image orientation and dense matching. Micmac determines automatically the optimal resolution of the orthophotography and the DEM from the dataset characteristics (images configuration and resolutions). In our experiment, the DEM was calculated on a 11cm grid (Figure 7). An orthophotography was also calculated with a 11cm pixel.

5 The independant set of 469 points located near the reservoir was used to compute estimation error. The following statistics have been retained: mean error, median of error, standard deviation of the error, and 90% confidence interval. They are reported in Table 3.

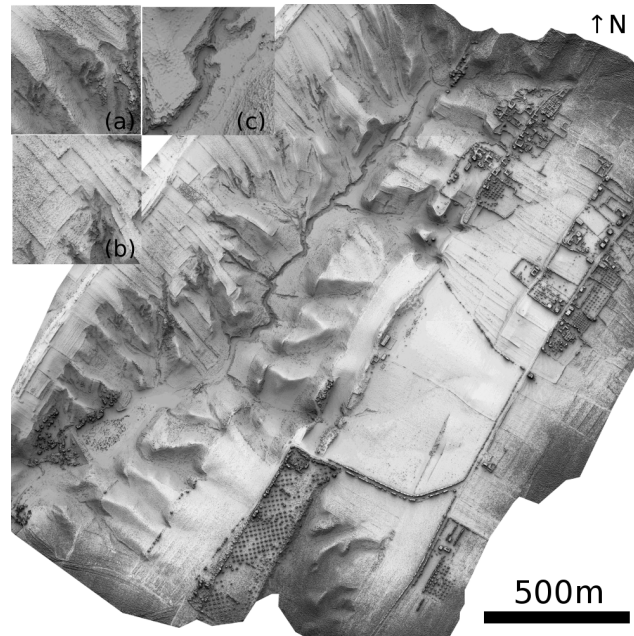


Figure 7. Shaded view of the computed DEM over the Kamech test site. (a) gully head ; (b) plots borders and a gully head ; (c) regressive erosion in the main thalweg

Table 3. DEM error statistics

Mean (m)	+0.06
Median (m)	+0.07
Standard deviation (m)	0.22
90% confidence intervall (m)	[-0.29 ; 0.81]
Sample size	469

3.3 Gullies mapping

A ~~deep~~ inspection of the shaded DEM alone (Figure 7) and of some of its detailed views already shows that DEM planimetric and altimetric resolution allows detection of numerous landscape features including all gully heads (e.g. subfigures 7-a and 7-b). The plots position and limits are also clearly depicted (subfigure 7-b). **Plot** limits form humps due to tillage erosion. In the thalweg (subfigure 7-c), marks of regressive erosion are visible. Finally, most ~~of~~ man-made structures are visible with topographic information at this scale: roads, tracks, buildings, plot limits. Apart from the method proposed above, it is hence reasonable to think that such detailed DEMs, with further processing, would allow the production of numerous thematic maps in the fields of hydrology, erosion, agronomy, geomorphology, etc...

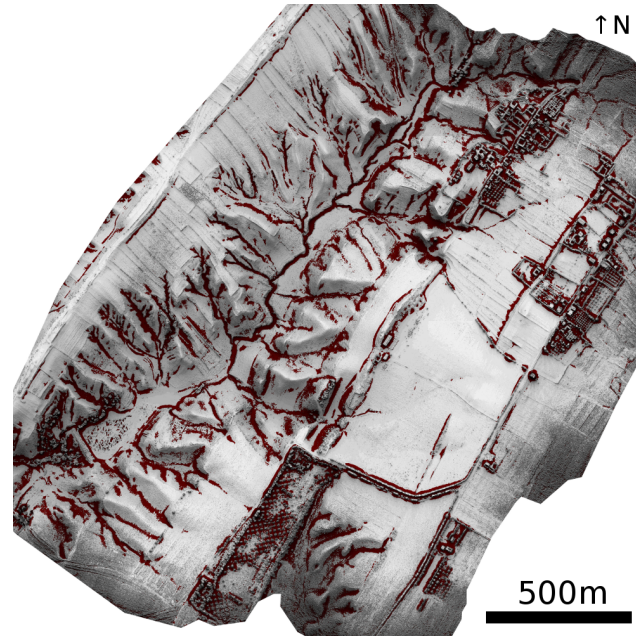


Figure 8. Raw result of the proposed gully detection algorithm

Full exploitation of such a rich topographic information goes beyond the scope of this article. The proposed gullies mapping method is only one example of its possible application in research. Figure 8 shows gullies mapped by the proposed method, superimposed on the shaded DEM. Apart from artefacts in inhabited areas, this map shows the potential of the proposed method for exhaustive gullies mapping within an area of several square kilometres. It can be observed that the test site comprises different kind of gullies. Some gullies (in the area showed on subfigure 7-a) remain contained in greater ravines and some gullies (in the area showed on subfigure 7-b) have a regressive dynamic and spread into cultivated plots.

4 Discussion

15 Effectiveness of image acquisition and processing

As reported by other authors (e.g. Verhoeven, 2009; Murray et al., 2013) , amongst the different issues caused by the use of a kite as a carrier for a camera, the effectiveness and correctness of flight plan realisation is probably the most critical. Moreover in our case - image acquisition for 3D modelling - the priority is to ensure a complete multi-view coverage of the area of interest. Apart from the experiment presented above, the method presented herein has also been successfully applied on another test site in Tunisia. El Maaoui et al. (2015) report an application of the method to cover more than 35 ha with images acquired at two different scales. Pictures were taken at two altitudes, which necessitated unrolling different line lengths during the flight. Stereo coverage was complete, allowing production of a seamless DEM for the targeted area.



For centuries now the potential of the kite as a platform was known. Kites were used as one of the first platforms for remote sensing. With the advent and the success of new technologies for easy production and processing of very high resolution imagery, kites came back into interest. As stated by Duffy and Anderson (2016), kites may experience a renewal of interest as an alternative to lightweight rotary wings UAVs.

DEM quality

For SfM applications in geosciences, a lot of authors express DEM quality in terms of quality of model geometry estimation. This is commonly measured by calculating a RMSE on GCPs. This expresses how well algorithms managed to fit the model to sparse point ground data given as an input. This figure can give some information about the quality of elevation estimation but only in a very indirect manner. Thematic applications and further processing of obtained DEMs necessitate having an idea of the quality of topography representation. In SfM application from very light platforms, this issue is quite a delicate one, for two main reasons. First, only few authors using kites present external validation of the estimated elevation data. Then, and more generally, DEM quality estimation is itself an ongoing research question. As raised by some authors (e.g. Lane, 2000), data quality and ways to qualify topographic data is a critical issue and, as pointed recently by Smith et al. (2016), this is all the more critical with a new and fast emerging technology.

Back to validation of high-resolution topographic data obtained by kites, ? do quality check by subtracting different DEMs and examining the detected terrain dynamics. These authors observe that feature characteristics (position, shape, size) are consistent with erosion processes and hence confirm the validity of their approach.

Several other authors perform quantitative validation with external data, with the same validation methods as the ones identified by Smith et al. (2016). A key point to keep in mind before comparing results of different studies is the fact that elevation estimation error is strongly correlated to the ground sampling distance. This is a well known characteristic in classical photogrammetry (e.g. Kraus and Waldhäusl, 1993) and is all the more true with multi-view SfM due to the high amount of images covering the same area. It is indeed not rare that a point is seen more than ten times.

Wundram and Loeffler (2008) use images with a 0.25m ground sampling distance and one thousand independent validation points. They achieve a 0.13m mean error, 0.36m standard deviation of the error and 0.75m maximal error. Smith et al. (2009) acquired images with an estimated 0.01-0.02m ground sampling distance. Error statistics obtained with 399 independent validation points is -0.01m for the mean error and 0.065m standard deviation error. Finally, El Maoui et al. (2015) computed a DEM with a ground sampling distance of 0.06m and assessed DEM quality with 176 independent validation points. Mean error is 0.04m and standard deviation of the error 0.07m.

These figures confirm that our results are in par with other works, both in terms of bias and dispersion. Mean error remains "within the pixel" ; in other words, observed bias is of the same order of magnitude as the ground sampling distance. Standard deviation of the error is also of the same order of magnitude as the ground sampling distance. It is hence shown that the proposed method allows topographic mapping on several kilometre square areas with decimetric resolution, both altimetric and planimetric.



Gullies mapping

10 With the advent of very high resolution topographic information, firstly from LiDAR, and now from SfM processing of high resolution images datasets, a lot of work aiming at deriving landscapes features can already be done, leading more recently to the release of dedicated open-source software, such as GeoNet (Sangireddy et al., 2016).

After having reviewed applications of such methods to the understanding of mass and energy transfer, Passalacqua et al. (2015) point out three characteristics of present and future work. Firstly, algorithms still hardly take advantage of the total amount of information that these new data represent. That is the case for our algorithm, which is a focal/local filtering of topography but still does not handle multiscale information for instance. Indeed, multiscale information has to be fully handled considering the impact of scale in such analyses (e.g. Tarolli and Fontana, 2009; Pirotti and Tarolli, 2010; Koenders et al., 2014). Secondly, further research has to be done on filtering/post-processing. Again, it is very clear in our results, and in the results of other authors (e.g. Tarolli and Fontana, 2009), that artificial objects present topographic characteristics similar to the ones of natural landmarks, with high curvatures and/or noticeable singularities. Finally, incertitude of the mapping results has to be estimated.

Additionally, as pointed by several authors, availability of very high resolution topographic information as obtained by our method allows for channel/feature extraction with focal processing, when classical methods with coarser DEMs required algorithms with global processing (Lashermes et al., 2007; Tarolli and Fontana, 2009; Passalacqua et al., 2015). This is all the more true when a part of classical algorithms are based on slope-area relationships and that the meaning of slope estimated from very fine DEMs is quite debatable (Tarolli and Tarboton, 2006).

When looking more closely at existing methods and algorithms, it can be seen that the approach proposed by Lashermes et al. (2007) shows interesting similarities with the one proposed above, in particular in the first part of their method, which implies, in a somehow comparable way, smoothing of topographic information. The two studies differ a lot in terms of study sites (a mountaneous area for these authors, and a hilly cultivated landscape here) and scales (a DEM sampled at 1m for these authors and at 0.11m here) and both have promising results, which indicates a high robustness of methods based on the use of smoothed topographic information. Moreover, these authors go a step further in the channel detection by linking the results obtained in the first step. This way, these authors produce a map of the full channel network.

A large part of the references in the literature deal with methods based on curvature analysis. With a view to assess potential of the LiDAR data, Tarolli and Fontana (2009) first looked at the impact of DEM resolution on curvature algorithms results and found that a resolution of 1m suits their needs for mapping landscape features in natural areas. This approach differs from the one proposed here, essentially due to the two characteristics of our problematic. Firstly, landscapes in cultivated hills of Tunisia can show nested forms of erosion, with new active gullies developing in older and bigger ravines. Secondly, another issue of such landscapes is the need for - ideally !- exhaustive and blind mapping, allowing for both understanding and management of erosion processing.

Then, and in line with the work of Tarolli and Fontana (2009), Pirotti and Tarolli (2010) proposed a method analysing curvatures computed on different windows sizes, on 1m DEMs derived from LiDAR point clouds with different densities.



10 Channels are detected by thresholding the curvature computed from these 1m DEMs. Even if some similarities can be found with our approach, smoothing is used here to explore the impact of LiDAR point density on channel detection. The work of these authors shows also that too rough curvature maps do not allow for proper channel extraction. Again, these authors highlight the critical importance of scale in DEM post-processing for feature detection.

5 Conclusions

15 In this work we proposed an alternative method to answer the issue of quasi-exhaustive mapping erosion features on kilometre square areas. This alternative lies on frugal innovation principles: reduce cost and complexity, without sacrificing quality (which substantially differs from low cost approaches, where quality is decreased). The proposed alternative addressed mainly the following points: acquisition costliness (namely, fixed-wing UAS and/or laser scanners) and difficult implementation of rotary wing UAVs (local regulations, weather conditions).

20 As a consequence we chose to assess the ability of kite platforms and consumer grade cameras to acquire images suitable for 3D analysis on kilometre square areas. We chose framed delta kites for their reliability and their easy use in field. With a view to realise appropriate flight plans - and without any downlink - we based our acquisition protocol on the fact that kites were steady relatively to the operator. Within these conditions, flight plans are realised and secured by the fact that the operator knows were to walk to put the camera on the expected flight tracks. This hypothesis - ~~admittedly~~ - was validated with
25 kite flight experimentations and simulations. We verified that kite effective flight angle was stable when used in the adapted wind conditions and with thin and light line. Moreover, the same method has been used on another site on which the projected flight plan was correctly accomplished.

Then, with correct flight plans, a dataset covering more than 3km² was acquired and processed in order to obtain a DEM with a resolution of 11cm. Altimetric quality of this DEM was assessed with more than four hundred independent validation
30 points. The estimated mean error is 0.06m and the estimated standard deviation of the error is 0.22m. Estimation bias of altitude falls therefore within pixel. Precision is of the order of magnitude of one pixel. Such results are on par with other works of the literature conducted on smaller areas.

Finally, we provided initial insights of harnessing the potential of such very high resolution DEMs produced on kilometre square areas. Visual examination of the DEM shows that all gully heads are clearly visible in the shaded model. We proposed a method for exhaustive gully mapping and applied this algorithm on our data. This allowed the mapping of different erosion features existing on our test site including gully erosion contained in larger inactive ravines and regressive erosion spreading into cultivated plots.

5 These results open a new window in the field of quantitative monitoring of natural disasters such as erosion in cultivated areas. The method proposed, developed with frugal innovation principles, has a solid potential to be spread, especially in developing countries where the issues about environmental resources urge scientists and managers to propose new solutions to map and monitor erosion. Due to the encouraging results obtained, it seems interesting to look deeper for future issues. First, if absolute cartographic precision is needed, implementation of the method still requires differential positioning, which is



expensive. Developing other ways to give a fair cartographic precision to tridimensionnal models is a promising issue. Minimal additional technological input would be required to improve the acquisition protocol ; for instance we could use a smartphone to check the operator's track during the flight. Finally, going deeper in the gullies mapping and analysis, by refining the proposed algorithm and/or comparing it to other existing algorithms would help to better assess the potential of this topographic data and understand erosion processes.

Competing interests. The authors declare that they have no conflict of interest.

Acknowledgements. The OMERE observatory (<http://www.obs-omere.org>), funded by the French institutes INRA and IRD and coordinated by INAT Tunis, INRGREF Tunis, UMR Hydrosociences Montpellier and UMR LISAH Montpellier, is acknowledged for providing a portion of the data used in this study. In particular, we gratefully acknowledge Kilani Ben Hazzez M'Hamdi, Radhouane Hamdi and Michael Schibler from IRD Tunis for the work realised in field to obtain topographic data.



References

- Aber, J. S., Marzloff, I., and Ries, J.: Small-format aerial photography: Principles, techniques and geoscience applications, Elsevier, 2010.
- Bird, S., Hogan, D., and Schwab, J.: Photogrammetric monitoring of small streams under a riparian forest canopy, *Earth Surface Processes and Landforms*, 35, 952–970, 2010.
- 15
- Bryson, M., Johnson-Roberson, M., Murphy, R. J., and Bongiorno, D.: Kite aerial photography for low-cost, ultra-high spatial resolution multi-spectral mapping of intertidal landscapes, *PLOS ONE*, 8, 2013.
- Campo-Bescós, M., Flores-Cervantes, J., Bras, R., Casali, J., and Giráldez, J.: Evaluation of a gully headcut retreat model using multitemporal aerial photographs and digital elevation models, *Journal of Geophysical Research: Earth Surface*, 118, 2159–2173, 2013.
- 20
- Duffy, J. P. and Anderson, K.: A 21st-century renaissance of kites as platforms for proximal sensing, *Progress in Physical Geography*, 40, 352–361, 2016.
- El Maoui, M., Feurer, D., Planchon, O., Boussema, M., and Snane, M.: Assessment of kite borne DEM accuracy for gullies measuring, *Journal of Research in Environmental and Earth Sciences*, 3, 118–124, 2015.
- Fonstad, M. A. and Marcus, W. A.: High resolution, basin extent observations and implications for understanding river form and process, *Earth Surface Processes and Landforms*, 35, 680–698, 2010.
- 25
- Fonstad, M. A., Dietrich, J. T., Courville, B. C., Jensen, J. L., and Carbonneau, P. E.: Topographic structure from motion: a new development in photogrammetric measurement, *Earth Surface Processes and Landforms*, 38, 421–430, 2013.
- Furukawa, Y. and Ponce, J.: Accurate, dense, and robust multi-view stereopsis, *IEEE Trans. on Pattern Analysis and Machine Intelligence*, 32, 1362–1376, 2010.
- 30
- Hancock, G. and Evans, K.: Channel head location and characteristics using digital elevation models, *Earth Surface Processes and Landforms*, 31, 809–824, 2006.
- Harwin, S. and Lucieer, A.: Assessing the accuracy of georeferenced point clouds produced via multi-view stereopsis from unmanned aerial vehicle (UAV) imagery, *Remote Sensing*, 4, 1573–1599, 2012.
- Hayas, A., Giráldez, J. V., Laguna, A., Peña, P., and Vanwalleghem, T.: Quantifying gully erosion contribution from morphodynamic analysis of historical aerial photographs in a large catchment SW Spain, *Earth Surface Processes and Landforms*, 17, 798, 2015.
- 35
- Jaud, M., Passot, S., Le Bivic, R., Delacourt, C., Grandjean, P., and Le Dantec, N.: Assessing the accuracy of high resolution digital surface models computed by PhotoScan® and MicMac® in sub-optimal survey conditions, *Remote Sensing*, 8, 465, 2016.
- Khalili, A. E., Raclot, D., Habaeib, H., and Lachère, J. M.: Factors and processes of permanent gully evolution in a Mediterranean marly environment (Cape Bon, Tunisia), *Hydrological Sciences Journal*, 58, 1519–1531, 2013.
- Koenders, R., Lindenbergh, R., Storms, J., and Menenti, M.: Multiscale curvatures for identifying channel locations from DEMs, *Computers & Geosciences*, 68, 11 – 21, 2014.
- 5
- Kraus, K. and Waldhäusl, P.: *Photogrammetry: Fundamentals and standard processes*, Photogrammetry, Dümmler, 1993.
- Lane, S.: The measurement of river channel morphology using digital photogrammetry, *Photogrammetric Record*, 16, 937–957, 2000.
- Lashermes, B., Fofoula-Georgiou, E., and Dietrich, W. E.: Channel network extraction from high resolution topography using wavelets, *Geophysical Research Letters*, 34, 2007.
- Lorenz, R. D. and Scheidt, S. P.: Compact and inexpensive kite apparatus for geomorphological field aerial photography, with some remarks on operations, *GeoResJ*, 3, 1–8, 2014.
- 10
- Lowe, D. G.: Distinctive image features from scale-invariant keypoints, *International Journal of Computer Vision*, 60, 91–110, 2004.



- Marzoff, I. and Poesen, J.: The potential of 3D gully monitoring with GIS using high-resolution aerial photography and a digital photogrammetry system, *Geomorphology*, 111, 48–60, 2009.
- 15 Mekki, I.: Analyse et modélisation de la variabilité des flux hydriques à l'échelle d'un bassin versant cultivé alimentant un lac collinaire du domaine semi-aride méditerranéen (Oued Kamech, Cap Bon, Tunisie), Ph.D. thesis, Montpellier 2, Université des Sciences et Techniques du Languedoc, 2003.
- Mekki, I., Albergel, J., Mechlia, N. B., and Voltz, M.: Assessment of overland flow variation and blue water production in a farmed semi-arid water harvesting catchment, *Physics and Chemistry of the Earth, Parts A/B/C*, 31, 1048–1061, 2006.
- Murray, J. C., Neal, M. J., and Labrosse, F.: Development and deployment of an intelligent Kite Aerial Photography Platform (iKAPP) for
20 site surveying and image acquisition, *Journal of Field Robotics*, 30, 288–307, 2013.
- Nachtergaele, J. and Poesen, J.: Assessment of soil losses by ephemeral gully erosion using high-altitude (stereo) aerial photographs, *Earth Surface Processes and Landforms*, 24, 693–706, 1999.
- Nex, F. and Remondino, F.: UAV for 3D mapping applications: a review, *Applied Geomatics*, 6, 1–15, 2014.
- Passalacqua, P., Belmont, P., Staley, D. M., Simley, J. D., Arrowsmith, J. R., Bode, C. A., Crosby, C., DeLong, S. B., Glenn, N. F., Kelly, S. A.,
25 Lague, D., Sangireddy, H., Schaffrath, K., Tarboton, D. G., Wasklewicz, T., and Wheaton, J. M.: Analyzing high resolution topography for advancing the understanding of mass and energy transfer through landscapes: A review, *Earth-Science Reviews*, 148, 174 – 193, 2015.
- Pierrot-Deseilligny, M. and Paparoditis, N.: A multiresolution and optimization-based image matching approach: An application to surface reconstruction from SPOT5-HRS stereo imagery, *Archives of Photogrammetry, Remote Sensing and Spatial Information Sciences*, 36, 2006.
- 30 Pirotti, F. and Tarolli, P.: Suitability of LiDAR point density and derived landform curvature maps for channel network extraction, *Hydrological Processes*, 24, 1187–1197, 2010.
- Raclot, D. and Albergel, J.: Runoff and water erosion modelling using WEPP on a Mediterranean cultivated catchment, *Physics and Chemistry of the Earth, Parts A/B/C*, 31, 1038–1047, 2006.
- Rango, A., Laliberte, A., Herrick, J. E., Winters, C., Havstad, K., Steele, C., Browning, D., et al.: Unmanned aerial vehicle-based remote
35 sensing for rangeland assessment, monitoring, and management, *Journal of Applied Remote Sensing*, 3, 033 542, 2009.
- Rengers, F. K. and Tucker, G. E.: The evolution of gully headcut morphology: a case study using terrestrial laser scanning and hydrological monitoring, *Earth Surface Processes and Landforms*, 40, 1304–1317, 2015.
- Sangireddy, H., Stark, C. P., Kladyk, A., and Passalacqua, P.: GeoNet: An open source software for the automatic and objective extraction of channel heads, channel network, and channel morphology from high resolution topography data, *Environmental Modelling & Software*, 83, 58 – 73, 2016.
- Smith, M. J., Chandler, J., and Rose, J.: High spatial resolution data acquisition for the geosciences: kite aerial photography, *Earth Surface
5 Processes and Landforms*, 34, 155–161, 2009.
- Smith, M. W., Carrivick, J. L., and Quincey, D. J.: Structure from motion photogrammetry in physical geography, *Progress In Physical Geography*, 40, 247–275, 2016.
- Snavely, N., Seitz, S. M., and Szeliski, R.: Photo tourism: exploring photo collections in 3D, in: *ACM transactions on graphics (TOG)*, vol. 25, pp. 835–846, ACM, 2006.
- 10 Stumpf, A., Malet, J.-P., Allemand, P., Pierrot-Deseilligny, M., and Skupinski, G.: Ground-based multi-view photogrammetry for the monitoring of landslide deformation and erosion, *Geomorphology*, 231, 130 – 145, 2015.



- Tarolli, P. and Fontana, G. D.: Hillslope-to-valley transition morphology: New opportunities from high resolution DTMs, *Geomorphology*, 113, 47 – 56, 2009.
- Tarolli, P. and Tarboton, D. G.: A new method for determination of most likely landslide initiation points and the evaluation of digital terrain model scale in terrain stability mapping, *Hydrology and Earth System Sciences*, 10, 663–677, 2006.
- Vandekerckhove, L., Poesen, J., and Govers, G.: Medium-term gully headcut retreat rates in Southeast Spain determined from aerial photographs and ground measurements, *Catena*, 50, 329–352, 2003.
- Vanmaercke, M., Poesen, J., Van Mele, B., Demuzere, M., Bruynseels, A., Golosov, V., Bezerra, J. F. R., Bolysov, S., Dvinskih, A., Frankl, A., et al.: How fast do gully headcuts retreat?, *Earth-Science Reviews*, 154, 336–355, 2016.
- 485 Verhoeven, G. J.: Providing an archaeological bird’s-eye view—an overall picture of ground-based means to execute low-altitude aerial photography (LAAP) in Archaeology, *Archaeological Prospection*, 16, 233–249, 2009.
- Westoby, M., Brasington, J., Glasser, N., Hambrey, M., and Reynolds, J.: ‘Structure-from-Motion’ photogrammetry: A low-cost, effective tool for geoscience applications, *Geomorphology*, 179, 300–314, 2012.
- 490 Wundram, D. and Loeffler, J.: High-resolution spatial analysis of mountain landscapes using a low-altitude remote sensing approach, *International Journal of Remote Sensing*, 29, 961–974, 2008.